A Flavin Cofactor-Binding PAS Domain Regulates c-di-GMP Synthesis in *Ax*DGC2 from *Acetobacter xylinum*[†]

Yaning Qi, Feng Rao, Zhen Luo, and Zhao-Xun Liang*

Division of Chemical Biology and Biotechnology, School of Biological Sciences, Nanyang Technological University, 60 Nanyang Drive, Singapore 637551

ABSTRACT: The cytoplasmic protein *Ax*DGC2 regulates cellulose synthesis in the obligate aerobe *Acetobacter xylinum* by controlling the cellular concentration of the cyclic dinucleotide messenger c-di-GMP. *Ax*DGC2 contains a Per-Arnt-Sim (PAS) domain and two putative catalytic domains (GGDEF and EAL) for c-di-GMP metabolism. We found that the PAS domain of *Ax*DGC2 binds a flavin adenine dinucleotide (FAD) cofactor noncovalently. The redox status of the FAD cofactor modulates the catalytic activity of the GGDEF domain for c-di-GMP synthesis, with the oxidized form exhibiting higher catalytic activity and stronger substrate inhibition. The results suggest that *Ax*DGC2 is a signaling protein that regulates the cellular c-di-GMP level in response to the change in cellular redox status or oxygen concentration. Moreover, several residues predicated to be involved in FAD binding and signal transduction were mutated to examine the impact on redox potential and catalytic activity. Despite the minor perturbation of redox potential and unexpected modification of FAD in one of the mutants, none of the single mutations was able to completely disrupt the transmission of the signal to the GGDEF domain, indicating that the change in the FAD redox state can still trigger structural changes in the PAS domain probably by using substituted hydrogen-bonded water networks. Meanwhile, although the EAL domain of *Ax*DGC2 was found to be catalytically inactive toward c-di-GMP, it was capable of hydrolyzing some phosphodiester bond-containing nonphysiological substrates. Together with the previously reported oxygen-dependent activity of the homologous *Ax*PDEA1, the results provided new insight into relationships among oxygen level, c-di-GMP concentration, and cellulose synthesis in *A. xylinum*.

The cyclic dinucleotide c-di-GMP[1] has emerged as a major signaling messenger in bacteria for regulating a variety of cellular functions and behaviors (*1, 2*). The cellular concentration of c-di-GMP is maintained by the proteins that contain the GGDEF, EAL, or HD-GYP domain (*3*). The GGDEF domains named after the conserved GGDEF motif function as diguanylate cyclases (DGCs) for c-di-GMP synthesis, whereas the EAL domains and HD-GYP domains characterized by the signature EAL or HD/GYP motifs function as phosphodiesterases (PDEs) for c-di-GMP hydrolysis (*2, 4, 5*). Many GGDEF, EAL, and HD-GYP domains are associated with putative sensor domains

for the perception of various environmental signals (*6, 7*). The characterization of the sensor domains and associated signals represents one of the major challenges in understanding c-di-GMP signaling. Considering that c-di-GMP controls phenotypes such as virulence expression and biofilm formation, the identification of the signals that regulate the cellular c-di-GMP level may also be crucial for understanding host–pathogen interaction and bacterial pathogenicity.

A large number of the putative sensor domains associated with GGDEF, EAL, and HD-GYP domains are the ubiquitous Per-Arnt-Sim (PAS) domains found in all kingdoms of life (*8, 9*). PAS domains are best known as sensor domains for the perception of changes in oxygen concentration, light intensity, voltage, and redox potential (*8, 10*). Several heme-containing PAS domains that sense gaseous ligands, including O_2, CO, and NO, have been characterized in detail (*8, 10–12*). For example, the heme-containing PAS domains of *Ax*PDEA1 and *Ec*Dos regulate the activity of the EAL domain by reversibly binding to O_2 (*13, 14*). The structural change in the PAS domain induced by O_2 binding can be transmitted to modulate the catalytic activity of the output domain. In addition to heme-binding PAS domains, two classes of flavin-binding PAS domains have been under intensive investigation in recent years. The first class, as represented by the BLUF and LOV photoreceptors, uses the flavin cofactor as a chromophore for sensing blue light (*15–19*). The isoalloxazine moiety of the flavin responds to photon activation by triggering structural change in the protein scaffold. The molecular mechanisms for the light-driven structural change vary among the PAS

[1]Abbreviations: 6-OH-FAD, 6-hydroxyl flavin adenine dinucleotide; *Ax*DGC2, DGC2 protein from *Acetobacter xylinum*; *Ax*PDEA1, PDEA1 protein from *A. xylinum*; Bis-*p*-Npp, bis(*p*-nitrophenyl) phosphate; BLUF, blue light receptor using FAD; c-di-GMP, cyclic di-GMP; EAL domain, EAL motif-containing c-di-GMP phosphodiesterase; DGC, diguanylate cyclase; *Ec*Dos, *Escherichia coli* Dos protein; FAD, flavin adenine dinucleotide; FMN, flavin mononucleotide; GGDEF domain, GGDEF motif-containing diguanylate cyclase; HD-GYP domain, C-di-GMP phosphodiesterase that contains the HD and GYP sequence motifs; HMWO, high-molecular weight oligomer; HPLC, high-performance liquid chromatography; LOV, light, oxygen, and voltage-sending PAS; PAS, Per-Arnt-Sim; PDE, phosphodiesterase; TFA, trifluoroacetic acid; thymidine-*p*-Npp, thymidine 5-monophosphate *p*-nitrophenyl ester.

domains, ranging from reversible formation of a covalent adduct between the flavin and a cysteine in LOV domains to reorganization of the hydrogen-bonded network in BLUF domains (15, 17). The second class of flavin-binding PAS domains perceives the change in oxygen tension or redox status in the surroundings, as exemplified by the PAS domains of *Azotobacter vinelandii* and *Klebsiella pneumonia* NifL, *Escherichia coli* Aer, and putatively *Methylococcus capsulatus* MmoS (20−22). Biochemical and structural studies of Aer and NifL have suggested that the change in the oxidation state of FAD would induce structural changes in the PAS domain and output domain (21, 23−25). It was also demonstrated that the FAD cofactor of *Kp*NifL can exchange electrons with menaquinone in *K. pneumonia*, suggesting that the menaquinone pool could be the physiological signal perceived by the PAS domain of *Kp*NifL (26). Since the reduced $FADH_2$ state can be rapidly oxidized by O_2, the PAS_{Aer} and PAS_{NifL} domains were also thought to function as indirect oxygen sensors. The observation of a putative oxygen channel in the crystal structure of PAS_{NifL} has provided further support for oxygen sensing (27).

Here we report the study of *Ax*DGC2, one of the proteins that regulate cellulose synthesis in the obligate aerobe *Acetobacter xylinum* (28). Although *Ax*DGC2 shares similar domain organization with two previously characterized heme-binding proteins *Ax*PDEA1 and *Ec*Dos (13, 29) (Figure 1), we demonstrate that the PAS domain of *Ax*DGC2 binds FAD as a cofactor instead and that the redox state of the flavin regulates the catalytic activity of the adjacent GGDEF domain for synthesizing c-di-GMP. Mutagenesis and kinetic measurement were used to probe the roles of several residues in cofactor binding and signal transduction. The results provided direct evidence for the role of the flavin-containing PAS domain as a redox or oxygen sensor. Together with the observed regulation of *Ax*PDEA1 by O_2 (13), the results also underscore the regulation of c-di-GMP concentration and cellulose synthesis by using both heme- and flavin-containing PAS domains for O_2 response in the obligate aerobe *A. xylinum*.

MATERIALS AND METHODS

Gene Cloning and Site-Directed Mutagenesis. The gene encoding *Ax*DGC2 from *A. xylinum* was obtained from Genscript and was ligated into the pET-26(b+) vector (Novagen) between compatible restriction sites. The resulting plasmid was used as a template for PCR amplification of the isolated EAL domain (*Ax*DGC2$_{306−574}$) with the primers 5′-AAACATA-TGCGCAATCTGCGTGAACG-3′ and 5′-AAACTCGAGCA-GGGTAACGC-3′. The Expanded High-Fidelity Kit (Roche) was used for PCR, and the amplified DNA fragments were also cloned into the pET-26(b+) vector between the compatible restriction sites. Site-directed mutagenesis was conducted using the Quik-Change mutagenesis kit (Stratagene) following the manufacturer's instructions. The sequences of the primers for mutagenesis are as follows: H62A mutation, 5′-CTGGTT-GGCAGCACCGCCCGCATTGTGAATAGCGG-3′ (forward primer) and 5′-CCGCTATTCACAATGCGGGCGGTGC-TGCCAACCAG-3′ (reverse primer); N66A mutation, 5′-GC-ACCCACCGCATTGTGGCTAGCGGCTATCATGATG-3′ (forward primer) and 5′-CATCATGATAGCCGCTAGCCA-CAATGCGGTGGGTGC-3′ (reverse primer); N94A mutation, 5′-CGCGGCAACATCTGTGCCCGTGCGAAAGATGGT-AG-3′ (forward primer) and 5′-CTACCATCTTTCGCAC-GGGCACAGATGTTGCCGCG-3′ (reverse primer); R125A
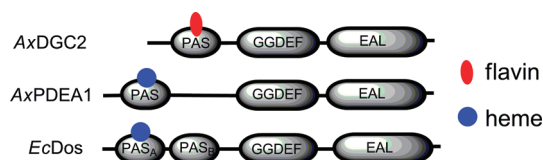

FIGURE 1: Comparison of the domain organization of the three PAS domain-containing proteins in c-di-GMP signaling (*Ax*DGC2 and *Ax*PDEA1 from *A. xylinum* and *Ec*Dos from *E. coli*).

mutation, 5′-CCGGCTATGTGGCGAGCGCCTTTGAAAT-TACCGAACT-3′ (forward primer) and 5′-AGTTCGGTAA-TTTCAAAGGCGCTCGCCACATAGCCGG-3′ (reverse primer); and D217A mutation, 5′-CTGACCCATCCGGA-TGCGCCGGTGAGCCGTCTG-3′ (forward primer) and 5′-CA-GACGGCTCACCGGCGCATCCGGATGGGTCAG-3′ (reverse primer).

Protein Expression and Purification. The plasmids harboring the genes were transformed into *E. coli* strain BL21(DE3) (Novagen). The cells were grown in Luria-Bertani (LB) medium at 37 °C with vigorous shaking (220 rpm) until the OD_{600} reached 0.6−0.8. Isopropyl β-D-thiogalactopyranoside (IPTG, 0.5 mM) was added to induce protein expression, and the culture was grown for an additional 16 h at 16 °C. Cells were harvested by centrifugation for 10 min at 5000 rpm. The cell pellet was frozen and thawed before the cells were lysed by sonication in 40 mL of lysis buffer [50 mM NaP$_i$ (pH 7.0)], 300 mM NaCl (200 mM for *Ax*DGC2$_{306−574}$), 5 mM mercaptoethanol (β-ME), 20 mM imidazole, 0.01% Triton X-100, and 0.2 mM phenylmethanesulfonyl fluoride (PMSF). The cell extract was centrifuged at 18000 rpm for 30 min. All the purification steps described below were performed at 4 °C. The supernatant was filtered and loaded onto 1 mL of Ni^{2+}-NTA resin (GE Healthcare) that had been prepacked into a column. The flow-through was collected and passed through the column again. The column was washed with 50 mL of washing buffer (lysis buffer supplemented with 50 mM imidazole). The proteins were eluted by using the elution buffer (lysis buffer supplemented with 300 mM imidazole). After sodium dodecyl sulfate−polyacrylamide gel electrophoresis (SDS−PAGE) gel analysis, fractions with a purity of >95% were pooled together and desalted by using either a PD-10 desalting column (GE Healthcare) or a Superdex 200 gel filtration column (GE Healthcare) with the AKTA FPLC system. The molecular weight of the proteins was estimated on the basis of the standard curve generated with the standards. The bright-yellow looking proteins were concentrated using an Amicon concentrator (Millipore) and were stored at −80 °C after the measurement of protein concentration by a Bradford assay. The typical protein yield for wild-type and mutant *Ax*DGC2 is 1−2 mg/L of culture. The final storage buffer was comprised of 50 mM Tris-HCl (pH 8.0), 50 mM NaCl, 5% glycerol, and 1 mM dithiothreitol (DTT).

Characterization of the Protein-Associated Flavin and c-di-GMP. A UV−vis spectrum was recorded using the UV-1650PC spectrophotometer (Shimadzu) equipped with thermostat and quartz cuvette. For HPLC analysis, *Ax*DGC2 was denatured with 1% TFA and the protein precipitate was removed by centrifugation. The yellow supernatant was loaded onto the Agilent LC1200 HPLC system column equipped with an XDB-C18 column (4.6 mm × 150 mm). The mobile phase is a gradient from 100% H_2O to 100% acetonitrile (with 0.045% TFA) over 100 min with a flow rate of 1 mL/min; 100 μM FMN and FAD

Scheme 1
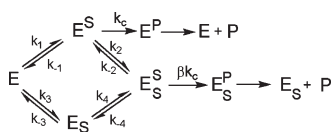
standards (Sigma) were also applied to the column using the same mobile phase. c-di-GMP bound by *Ax*DGC2 and its truncated construct were analyzed in the same fashion by HPLC.

Enzymatic Assay of DGC Activity. The progress of c-di-GMP synthesis catalyzed by the diguanylate cyclase domain of *Ax*DGC2 was monitored by using the Agilent LC1200 system [mobile phase of 20 mM triethylammonium bicarbonate (pH 7.0) and 9% methanol, at a rate of 1 mL/min] with an XDB-C18 column (4.6 mm × 150 mm). The enzymatic reaction was performed by incubating the enzyme and GTP (Sigma) at 23 °C in 100 mM Tris-HCl (pH 8.0), 50 mM KCl, and 10 mM MgCl$_2$. The reaction was stopped by adding $^1/_{20}$ reaction volume of 0.5 M EDTA and then boiled at 95 °C for 5 min. Following centrifugation at 14000 rpm for 5 min to remove the protein aggregate, the supernatant was filtered and loaded onto the HPLC system. Anaerobiosis was established in a Coy anaerobic chamber with the anaerobic buffer flushed with nitrogen for 0.5−1 h. The reduced form of *Ax*DGC2 was generated via addition of 2 mM sodium dithionite (Sigma) to the protein solution under anaerobic conditions. The redox reaction was monitored spectroscopically, and the fully reduced sample was mixed with an equal volume of oxygen-saturated buffer and exposed to air to reoxidize the protein. The oxidized and reduced *Ax*DGC2 were incubated with various concentrations of GTP, and the initial velocities were obtained from a series of reactions with different incubation times. The total turnover was controlled to ensure the accurate measurement of initial velocities within the linear range. The turnover number (k_{cat}) and Michaelis−Menten constant (K_M) were obtained by fitting the initial velocities at various substrate concentrations to the Michaelis−Menten equation with the exception of the proteins that exhibit substrate inhibition in the 0−300 μM GTP range. The kinetic data for these proteins were fit using a model that assumes the substrate binds to the enzyme at a productive and a nonproductive (or inhibitory) binding site (Scheme 1).

The curves were obtained by fitting the kinetic data to eq 1 derived from the model given above with steady-state and rapid equilibrium assumptions.

$$V = \frac{V_{max}(1/K_m + \beta[S]/\alpha K_i K_m)}{1/[S] + 1/K_m + 1/K_i + [S]/\alpha K_m K_i} \tag{1}$$

where K_i is the inhibition constant and α and β are the factors by which the K_M, K_i, and V_{max} change when the second substrate is bound at the nonproductive site.

Enzymatic Assay of PDE Activity. c-di-GMP was synthesized using the thermophilic DGC enzyme described previously (*30*). The reaction conditions for the phosphodiesterase assay included 100 mM Tris-HCl (pH 8.0), 25 mM KCl, and 10 mM MgCl$_2$ or MnCl$_2$. The buffer used for the five nonphysiological substrates [thymidine 5-monophosphate *p*-nitrophenyl ester sodium salt (thymidine-*p*-NPP), *O*-(4-nitrophenylphosphoryl)choline, bis(*p*-nitrophenyl) phosphate sodium salt (Bis-*p*-NPP), 4-nitrophenyl phosphate disodium salt hexahydrate, and phosphoenolpyruvic acid monopotassium salt] was 50 mM Tris-HCl (pH 8.0) with 25 mM MgCl$_2$. The reaction was monitored

spectroscopically, and the OD reading at 410 nm was recorded. For both thymidine-*p*-NPP and Bis-*p*-NPP, the measurement of the steady-state kinetic parameters was taken by monitoring the OD reading at 410 nm with a UV spectroscope. The kinetic parameters were obtained by fitting the initial velocities at various substrate concentrations to the Michaelis−Menten equation using Prism (GraphPad).

Measurement of the FAD:Protein Binding Stoichiometry. The protein concentration was measured by the Bradford method, whereas the content of the FAD was measured following the release the cofactor from the protein by acid denaturation and the concentration determined by using a molar extinction coefficient of free FAD at 450 nm of 11.3 mM^{-1} cm^{-1}. The concentration of the 6-hydroxyl FAD was determined using an extinction coefficient of 22.6 mM^{-1} cm^{-1} at 427 nm (*31*). The FAD:protein stoichiometry was obtained from the FAD to protein ratio.

Determination of the Redox Potential of Flavin in AxDGC2. The redox potentials of *Ax*DGC2 and its mutants were determined with the established method recently described by Ukaeglu et al. (*25*). Briefly, a 200 μL solution of 5−10 μM *Ax*DGC2 in 50 mM Tris-HCl (pH 8.0) was incubated anaerobically with 5 μM phenosafranin (Sigma) as a redox indicator at room temperature. A stock solution of 30 mM sodium dithionite was added in 1 μL aliquots inside the anaerobic chamber. The concentrations of oxidized and reduced *Ax*DGC2-bound FAD and phenosafranin were measured after each dithionite addition by monitoring the absorbance of FAD at 450 nm (H62A at 427 nm) and phenosafranin at 522 nm using the UV−vis spectrophotometer. The redox potential was determined by plotting log(Ox/Red) phenosafranin versus log(Ox/Red) *Ax*DGC2.

Structural Modeling. The structural model of the PAS$_{AxDGC2}$ domain was constructed using the Swiss-Model Server (*32*). The crystal structure of the PAS-A domain of MmoS [Protein Data Bank (PDB) entry 3ewk] was used as a template (*22*).

RESULTS

AxDGC2 Binds the FAD Cofactor in the PAS Domain. Approximately 20−30% of the recombinant *Ax*DGC2 was expressed as a soluble protein and purified by metal affinity and size-exclusion chromatography. The protein was found in two major fractions after being eluted from the gel exclusion column, with a yellow dimeric fraction and a colorless high-molecular weight oligomer (HMWO) fraction in the void volume. The absorption spectrum of the dimeric fraction suggested that the protein binds an oxidized flavin (FAD or FMN) cofactor, with the characteristic absorbance of 375, 450, and 470 nm for flavin-binding proteins (Figure 2 and Table 1). The flavin cofactor was dissociated from the protein after heat or trifluoroacetic acid (TFA) treatment, suggesting that the cofactor is noncovalently bound by the protein. The cofactor was confirmed to be FAD by comparison with the standard by HPLC as well as MALDI-MS analysis (MW of 787.1) (Figure 2, inset). The colorless HMWO fraction did not exhibit enzymatic activity, and thus, only the dimeric protein was further investigated. The FAD:protein stoichiometry for the dimeric form was measured to be 0.41 ± 0.1, indicating relatively weak affinity of the PAS domain for the cofactor. A few residues for flavin binding were predicted by comparison of the sequence with other flavin-binding PAS domains. We mutated a highly con-
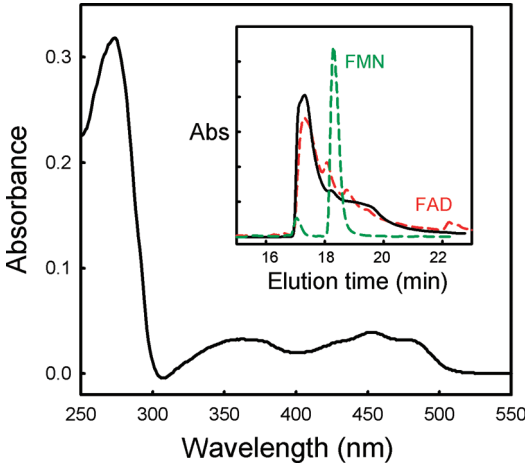
FIGURE 2: Absorption spectrum of *Ax*DGC2. The inset shows the HPLC analysis of the cofactor bound by *Ax*DGC2: denatured *Ax*DGC2 sample (black line), FAD standard (red dashed line), and FMN standard (green dashed line).

Table 1: Maxima of Absorption Spectra of Riboflavin-Containing PAS Proteins[a]

protein	cofactor	wavelength (nm)
*Ax*DGC2	FAD	375, 451, 480
*Av*NifL	FAD	358, 372, 446, 470
Aer	FAD	375, 450, 470
MmoS(PAS-A)	FAD	376, 444, 470
BLUF_AppA(light state)	FAD	367, 384, 457, 483
BLUF_AppA(dark state)		363, 378, 443, 471
LOV(NPH1)	FMN	380, 430, 450, 470

[a]*Ax*DGC2 from *A. xylinum*, AvNifL from *Az. vinelandii* (*24*), Aer from *E. coli* (*58*), MmoS from *M. capsulatus* (*25*), BLUF_Appa from *Synechocystis* sp. PCC6803 (*59*), and LOV-NPH1 from *Arabidopsis thaliana* (*15*).

served residue (Asn[94]) that putatively interacts with the isoalloxazine ring of FAD. The N94A mutant was purified as a FAD-free protein with a colorless appearance, confirming that the FAD is bound by the PAS domain.

*Ax*DGC2 contains two putative catalytic domains (GGDEF and EAL) for c-di-GMP synthesis and degradation, respectively. HPLC analysis of the extract from the denatured protein solution revealed another small ligand bound by the protein in addition to FAD. The small ligand was identified to be c-di-GMP by comparison with the standard using HPLC (Figure S1). c-di-GMP is most likely to be bound by the GGDEF domain because the presence of an inhibitory site (I-site) for c-di-GMP binding is well-known for the GGDEF domain (*30*, *33*, *34*). Sequence alignment showed that a few key residues, including one of the Arg residues for c-di-GMP binding in the I-site, are not conserved in *Ax*DGC2 (Figure S2 of the Supporting Information). To test whether c-di-GMP is indeed bound at the I-site, we mutated a conserved residue (Asp[217]) in the putative I-site. HPLC analysis of the denatured protein solution of mutant D217A showed that the protein was no longer associated with c-di-GMP (Figure S1 of the Supporting Information), suggesting that the GGDEF domain of *Ax*DGC2 contains an intact I-site even though the residues are not strictly conserved.

Regulation of DGC Activity by the Oxidation State of FAD. Enzymatic assays revealed that *Ax*DGC2 exhibited DGC activity by converting GTP to c-di-GMP when incubated with GTP and Mg^{2+}. In contrast, *Ax*DGC2 did not degrade c-di-
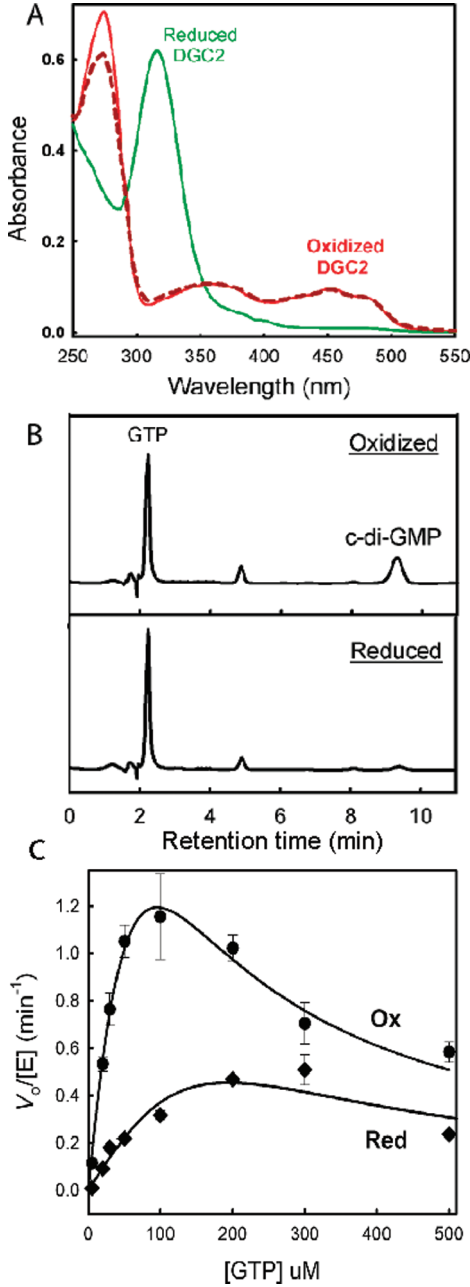

FIGURE 3: Regulation of DGC activity by the redox status of *Ax*DGC2. (A) The spectrum of reduced *Ax*DGC2 (green line) was recorded after incubation of oxidized *Ax*DGC2 (red solid line) with sodium dithionite. The spectrum of reoxidized *Ax*DGC2 (red dashed line) was recorded after reduced *Ax*DGC2 had been mixed with an equal volume of oxygenated buffer and exposed to air for 30 min. (B) HPLC analysis of product formation for oxidized and reduced *Ax*DGC2. Reaction conditions: 100 mM Tris-HCl (pH 8.0), 50 mM KCl, 10 mM $MgCl_2$, and 10 μM GTP. (C) Initial rate measurement for oxidized and reduced *Ax*DGC2. Reaction buffer consisted of 100 mM Tris-HCl (pH 8.0), 50 mM KCl, and 10 mM $MgCl_2$.

GMP even after prolonged incubation of the protein with c-di-GMP and Mg^{2+} or Mn^{2+}. Because some flavin-containing PAS domains function as photoreceptors for the perception of blue light and regulation of the activity of output domains, enzymatic assays were performed to test whether the PAS domain of *Ax*DGC2 functions as a photoreceptor; the protein was illuminated for 10−15 min using a continuous light source, and the absorption spectrum was immediately recorded. Unlike the BLUF and LOV domain-containing proteins, the absorption

Table 2: FAD:Protein Stoichiometry and Steady-State Kinetic Parameters for *Ax*DGC2 and Its Mutants[a]

enzyme	FAD:protein stoichiometry	redox state	k_{cat} (min^{-1})	K_M (μM)	k_{cat}/K_M (min^{-1} μM^{-1})	K_i (μM)
wild type	0.4	oxidized	5.6 ± 2.4	176 ± 89	$(3.2 \pm 2.1) \times 10^{-2}$	52 ± 27
		reduced	0.71 ± 0.1	112 ± 18	$(0.6 \pm 0.1) \times 10^{-2}$	$-;$
H62A	0.1	oxidized	7.2 ± 4.2	138 ± 106	$(5.2 \pm 5.0) \times 10^{-2}$	157 ± 135
		reduced	1.7 ± 0.4	196 ± 97	$(0.9 \pm 0.5) \times 10^{-2}$	$-;$
N66A	0.68	oxidized	2.8 ± 0.8	60 ± 29	$(4.7 \pm 2.7) \times 10^{-2}$	371 ± 233
		reduced	1.0 ± 0.5	189 ± 112	$(0.5 \pm 0.4) \times 10^{-2}$	50 ± 31
N94A	$-$	$-$	1.5 ± 1.3	239 ± 237	$(0.6 \pm 0.8) \times 10^{-2}$	38 ± 37
R125A	0.3	oxidized	8.0 ± 3.0	117 ± 59	$(6.9 \pm 4.4) \times 10^{-2}$	138 ± 77
		reduced	0.62 ± 0.1	107 ± 20	$(0.5 \pm 0.1) \times 10^{-2}$	$-;$

[a]Reaction conditions: 100 mM Tris-HCl (pH 8.0), 50 mM KCl, and 10 mM MgCl$_2$ at 23 °C.

spectrum of *Ax*DGC2 did not exhibit any noticeable change upon illumination. Moreover, enzymatic assays performed under the light and dark conditions showed that the rate of c-di-GMP synthesis was not altered, and that the EAL domain remained inactive under the light conditions. The light-independent catalytic activity of *Ax*DGC2 suggested that the PAS domain is not involved in light sensing.

Further enzymatic assays were conducted to test whether the redox status of the FAD cofactor modulates the catalytic activity of the GGDEF or EAL domain. The FAD cofactor in *Ax*DGC2 was readily reduced by sodium dithionite under anaerobic conditions. The complete conversion of the oxidized FAD to the reduced form was evident from the changes in the absorption spectrum, with the disappearance of the characteristic 451 and 480 nm peaks (Figure 3A). Reduced *Ax*DGC2 underwent rapid oxidation upon being exposed to the air as evidenced by the recovery of the absorption spectrum for the oxidized FAD. Such a reversible oxidation−reduction process has been documented for the PAS domains of Aer, NifL, and MmoS (20, 21, 25). To examine the catalytic activity of oxidized and reduced *Ax*DGC2, we prepared the reduced protein in an anaerobic chamber by incubating the protein with sodium dithionite, whereas we prepared the oxidized *Ax*DGC2 by exposing the reduced protein to air to ensure that the concentrations of the reduced and oxidized enzymes remain identical. Neither the oxidized nor the reduced *Ax*DGC2 could degrade c-di-GMP, suggesting the EAL domain remains inactive regardless of the redox status of the flavin. In contrast, the incubation of GTP and Mg^{2+} with the enzyme revealed that oxidized *Ax*DGC2 exhibited a higher efficiency than the reduced protein in synthesizing c-di-GMP (Figure 3B). Steady-state kinetic measurements were subsequently taken to characterize the activity of the oxidized and reduced *Ax*DGC2. The results showed that the oxidized form not only exhibited a higher catalytic rate but also displayed much stronger substrate inhibition in the 0−500 μM GTP range (Figure 3C). Comparison of the kinetic parameters revealed a 7.8-fold greater k_{cat} and an inhibition constant K_i of 52 ± 27 μM for the oxidized form (Table 2). Measurement of the kinetic parameters for oxidized *Ax*DGC2 in oxygenated or anaerobic buffer did not seem to affect the activity of the oxidized protein, indicating that the difference in catalytic activity is not due to the presence of O$_2$. To further confirm that the low catalytic activity for the reduced form was not due to the inhibition of sodium dithionite, we used the xanthine oxidase/xanthine/benzyl viologen system to reduce *Ax*DGC2 instead (35). The FAD of *Ax*DGC2 could be readily reduced by the enzyme system, and the oxidized *Ax*DGC2 still exhibited higher catalytic activity (Figure S3 of the Supporting Information). Moreover, the

presence of sodium dithionite did not affect the catalytic activity of the FAD-free mutant N94A (Figure S4 of the Supporting Information). Taken together, these results strongly suggest that the change in catalytic activity is caused by the oxidation and reduction of the FAD cofactor.

Effect of Mutations in the PAS Domain on DGC Activity. The PAS$_{AxDGC2}$ domain shares sequence identity and similarity with the PAS domains of Aer, *Kp*NifL, *Av*NifL, and MmoS (Figure 4A). In particular, the sequence of PAS$_{AxDGC2}$ is significantly identical (45%) and similar (76%) to that of the PAS$_{MmoS}$ domain. The high degree of sequence homology between PAS$_{AxDGC2}$ and PAS$_{MmoS}$ (PDB entry 3ewk) allowed us to build a reasonably reliable structural model for the PAS domain. Some of the key residues in *Av*NifL and Aer for the propagation of structural changes have been identified on the basis of structural and mutagenesis studies (27, 36). Moreover, the crystal structure of PAS$_{AvNifL}$ determined by Moffat and co-workers revealed a hydrogen-bonded network formed by residues Glu[70], Ser[39], His[133], and two water molecules in the proximity of the N5 atom of the FAD isoalloxazine ring. Interestingly, although the main residue (Asn[94]) crucial for FAD binding is conserved in PAS$_{AxDGC2}$, the residues near the N5 atom that may play important roles in signal propagation seem to be different from those of PAS$_{AvNifL}$ (27).

According to the structural model of PAS$_{AxDGC2}$, the residue Asn[94] directly interacts with the isoalloxazine moiety of FAD via hydrogen binding (Figure 4C). This residue is highly conserved in flavin-binding PAS domains, and it has been shown that the mutation of the equivalent residue in Aer resulted in an altered phenotype in *E. coli* (20). We found that the mutation of Asn[94] abolished binding of FAD to *Ax*DGC2, as evidenced by the colorless appearance of the protein and the absence of the FAD spectrum (Figure 5A). An enzymatic assay showed that the N94A mutant converted GTP to c-di-GMP with a k_{cat} that is 3.8-fold smaller than that of *Ax*DGC2. (Figure 5B and Table 2). In addition, the structural model suggested that residue Asn[66] is likely to form hydrogen bonds with the 2′-OH group or the ribityl chain and the O2 atom of the isoalloxazine ring. Surprisingly, the N66A mutant exhibited a higher FAD:protein stoichiometry (0.7 ± 0.1) than the wild type (0.41), suggesting Asn[66] is not as important as Asn[94] in binding the cofactor.

It has been proposed that the change in flavin redox state induces structural changes in PAS$_{AvNifL}$ via reorganization of the hydrogen-bonded network in the flavin-binding pocket, and that the reorganization of the hydrogen-bonded network is initiated by the protonation and deprotonation of the N5 atom of the isoalloxazine ring (27, 37). The structural model of PAS$_{AxDGC2}$ suggests that His[62] and Arg[125] are located near the N5 atom and
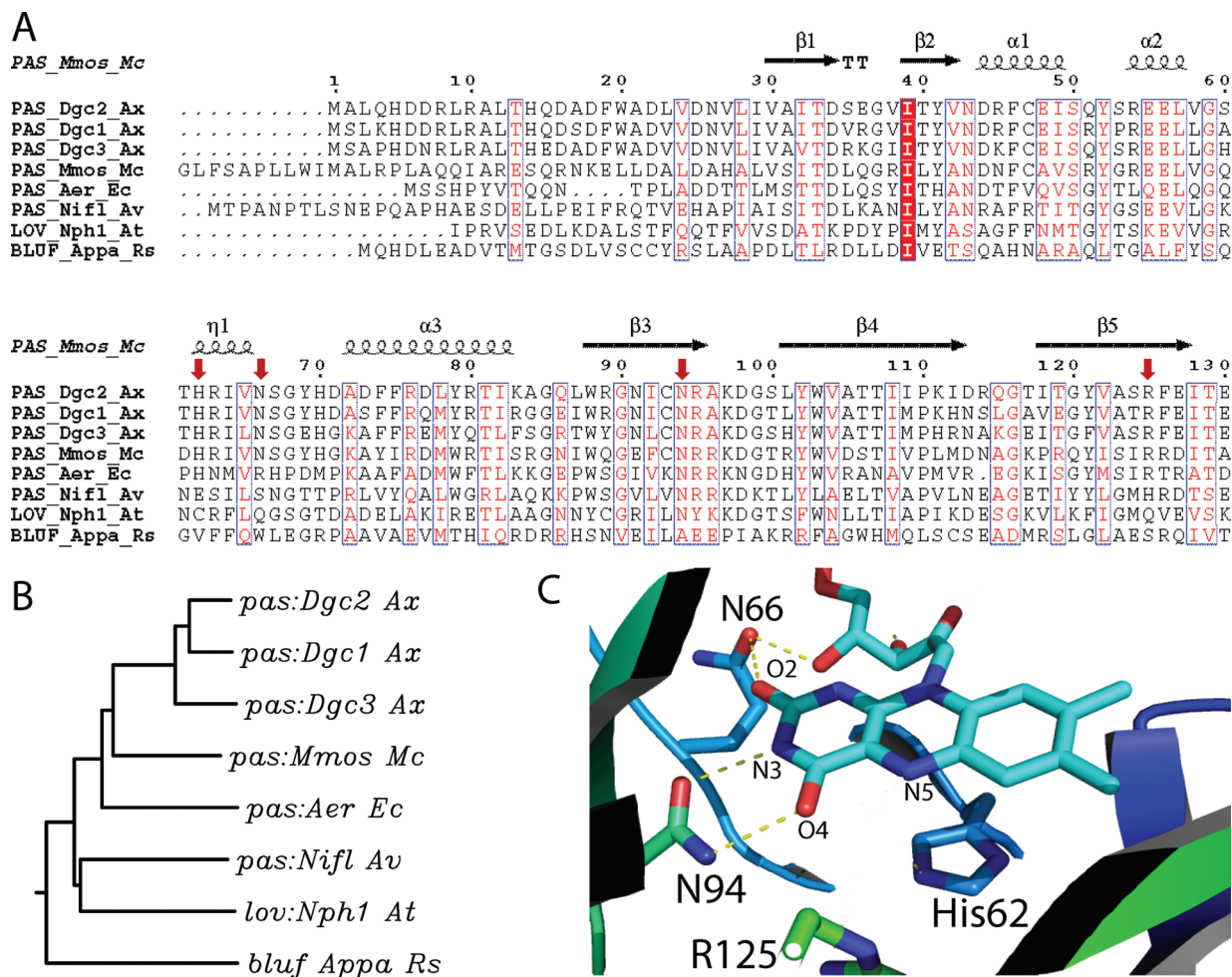
FIGURE 4: Comparison of the PAS$_{AxDGC2}$ domain with other flavin-binding PAS domains. (A) Sequence alignment of flavin-binding PAS domains. The four residues examined in this study are indicated by the arrows. (B) Phylogenetic relationship analysis of the PAS domains: AxDGC2 from *A. xylinum*, NifL from *Az. vinelandii* (*24*), Aer from *E. coli* (*58*), MmoS from *M. capsulatus* (*25*), BLUF_Appa from *Synechocystis* sp. PCC6803 (*59*), and LOV-NPH1 from *Ar. thaliana* (*15*). (C) Structural model of the PAS$_{AxDGC2}$ domain with the isoalloxazine ring and the four residues examined shown as sticks. The putative hydrogen bonds between the isoalloxazine ring and the residues are represented by dashed lines.

are the most likely participants in the formation of hydrogen bonds with N5 through one or more water molecules (Figure 4C). To assess their roles in signal transduction, the two residues were mutated individually for spectroscopic and kinetic characterization. The FAD:protein stoichiometry for the H62A and R125A mutants was measured to be 0.1 ± 0.03 and 0.3 ± 0.1 respectively. While the R125A mutation exhibited an absorption spectrum similar to that of the wild-type protein, the absorption spectrum of the H62A mutant has been changed drastically, suggesting either an altered binding environment or modified FAD (Figure 6A). To test whether the FAD has been modified, we denatured the mutant protein and found that the free cofactor indeed exhibited an altered retention time and absorption spectrum (Figure 7). A survey of the literature suggested that the modified FAD is most likely to be the neutral form of 6-hdyroxyl FAD (6-OH-FAD). 6-OH-FAD is known to occur naturally in several enzymes with a signature peak at ~430 nm and a broad peak (~600 nm, for the anionic form at high pH) (*31*, *38*, *39*). Despite the modification, the H62A mutant could still be readily reduced by sodium dithionate or the xanthine oxidase system. Enzymatic assays revealed that the oxidized forms of the R125A ad H62A mutants exhibited substrate inhibition similar to that of the wild-type protein and exhibited k_{cat} values 12.9- and 4.2-fold greater than those of their reduced

forms, respectively, relative to the 7.8-fold difference for *Ax*DGC2 (Figure 6B,D). Meanwhile, the oxidized and reduced forms of the N66A mutant still exhibited a difference of 2.8-fold in k_{cat} (Figure 6C). It should be noted, however, that the comparison of the differences in catalytic rate between the wild type and mutants is complicated by the different FAD:protein stoichiometry.

Effect of Mutations in the PAS Domain on Redox Potential. In *A. xylinum* cells, the FAD cofactor of *Ax*DGC2 is presumably oxidized by O_2 and reduced by an unknown partner via electron transfer. The rate of electron transfer, which could be crucial for the physiological function of the cofactor, is dependent on the redox potential and reorganization energy of the protein-embedded cofactor (*40–42*). To investigate the roles of the residues in modulating redox potential, we measured the oxidation potential of *Ax*DGC2 and its mutants (Figure S5 of the Supporting Information and Table 3). Wild-type *Ax*DGC2 exhibits a redox potential of -280 ± 3.0 mV, whereas mutants N66A and R125A exhibit slightly higher redox potentials of -275 ± 0.8 and -272 ± 2.2 mV, respectively. The H62A mutant that contains the modified FAD exhibited a higher potential of -265 ± 1.3 mV, which matches the potential of -265 mV measured for a 6-OH-FAD reconstituted ferredoxin-NADP$^+$ reductase (*43*). Overall, the redox potentials are lower compared
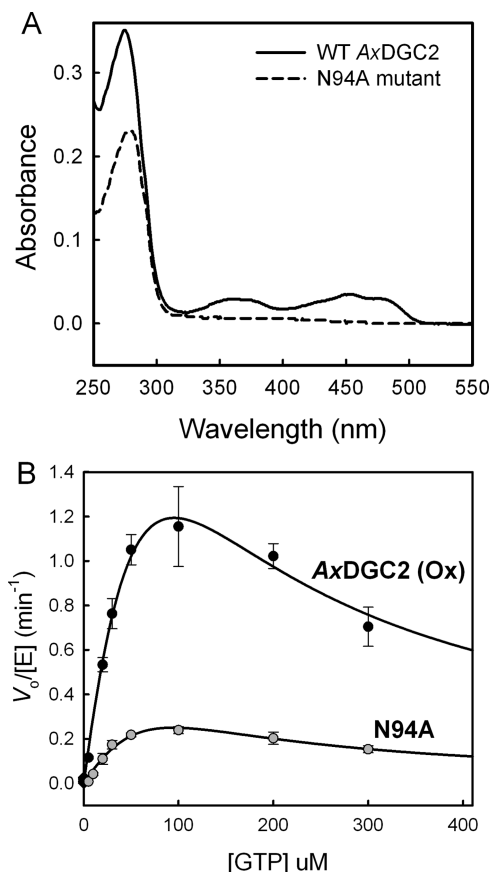
FIGURE 5: Comparison of *Ax*DGC2 and the N94A mutant. (A) Absorption spectra of *Ax*DGC2 and the N94A mutant. (B) Comparison of the catalytic activity of *Ax*DGC2 and the N94A mutant. Reaction buffer consisted of 100 mM Tris-HCl (pH 8.0), 50 mM KCl, and 10 mM MgCl$_2$.

to these of the free flavin (-220 mV) and *Av*NifL (-227 mV) but comparable to the potentials of -290 mV for MmoS and -277 mV for *Kp*NifL.

Phosphodiesterase Activity of the EAL Domain. The EAL domain of *Ax*DGC2 lacks a conserved loop 6 [DFG(T/A)-GYSS] found in catalytically active EAL domains (*44*). Instead, it contains a highly degenerate loop 6 consisting of N[473]FGK-GITVL[481]. We recently found that the restoration of the loop of the isolated EAL domain via mutation of three (N473D, K476T, and I478Y) residues is sufficient to recover the enzymatic activity of the domain in hydrolyzing c-di-GMP (*44*). Although the oxidized and reduced forms of *Ax*DGC2 did not hydrolyze c-di-GMP, wild-type *Ax*DGC2 could hydrolyze the nonphysiological phosphodiesterase substrates thymidine-*p*-NPP and Bis-*p*-NPP, but not the phosphatase substrates 4-nitrophenyl phosphate, *O*-(4-nitrophenylphosphoryl)choline, and phosphoenolpyruvic acid. Steady-state kinetic measurements showed that V_{max} was reached for thymidine-*p*-NPP at a millimolar substrate concentration, while no saturation was observed for the structurally simpler bis-*p*-NPP at a comparable substrate concentration (Figure 8A). *Ax*DGC2 was further found to be able to hydrolyze 2′,3′-cyclic AMP (cAMP) and 2′,3′-cyclic GMP (cGMP), two nonphysiological cyclic nucleotides (Figure 8B). The isolated EAL domain also exhibited similar activity toward the nonphysiological substrates, but not c-di-GMP. In addition, we confirmed that the catalytic activity of the EAL domain is independent of the FAD redox state (Figure S6 of the Supporting Information).

DISCUSSION

The cellulose-producing bacterium *A. xylinum* has been a model system for studying cellulose biosynthesis in bacteria. Cellulose synthesis is regulated by the reversible binding of the messenger c-di-GMP to a subunit of the cellulose synthesizing machinery (*45, 46*). Six homologous proteins (*Ax*PDEA1, -2, and -3 and *Ax*DGC1, -2, and -3) were found to control the cellular concentration of c-di-GMP in *A. xylinum* (*28*). Although the six proteins share a similar domain organization with a PAS-GGDEF-EAL arrangement, in vivo analysis suggested that *Ax*PDEA1, -2, and -3 are responsible for the degradation of c-di-GMP whereas *Ax*DGC1, -2, and -3 for c-di-GMP synthesis (*28*). It was also found that the binding of O$_2$ by the heme cofactor of the PAS domain of *Ax*PDEA1 suppresses the activity of the EAL domain, implying that high O$_2$ tension would retard the hydrolysis of c-di-GMP and lead to a higher c-di-GMP concentration (*13*). Despite the similar domain composition shared by *Ax*DGC2 and *Ax*PDEA1, the results from our study revealed several major differences between the two proteins. First, the PAS$_{Ax\text{DGC2}}$ domain binds FAD, in contrast to the heme cofactor in *Ax*PDEA1. This observation is consistent with the highest degree of sequence similarity shared by PAS$_{Ax\text{DGC2}}$ and the PAS domains of MmoS, Aer, and NifL. Second, *Ax*DGC2 contains a catalytically inactive EAL domain, whereas *Ax*PDEA1 contains a catalytically active EAL domain, consistent with the observation from in vivo studies and the mutations in a functional loop (*28, 44*). Third, while a high O$_2$ concentration stimulates the activity of the GGDEF domain of *Ax*DGC2 for c-di-GMP synthesis, it represses the EAL domain of *Ax*PDEA1 for c-di-GMP degradation.

The mutagenesis studies not only confirmed that Asn[94], but not Asn[66], is indispensible for FAD binding but also probed the roles of residues His[62] and Arg[125] in propagating the redox signal from FAD to the surrounding protein scaffold. Recent studies have suggested that the reversible protonation of the N5 atom of the isoalloxazine ring initiates the structural change in the FAD-containing *Av*NifL and BLUF through hydrogen-bonded networks (*27, 37*). Arg[125] is located near the N5 atom of the isoalloxazine ring and may affect the protonation and deprotonation of the N5 atom, whereas His[62] stacks on the isoalloxazine ring and may or may not form a hydrogen bond with N5 through water molecules. Importantly, the site in which His[62] resides is occupied by an essential cysteine residue that forms a covalent adduct with the FAD upon light irradiation in the light-sensing LOV domain (*47*) and is occupied by a Glu residue that plays a critical role initiating the reorganization of the hydrogen-bonded network in *Av*NifL (*27*). Our results showed that although the two single mutations caused some minor changes in redox potential and catalytic activity, they did not completely disrupt the transmission of the structural change to the GGDEF domain, which would be manifested by redox-independent DGC activity. The observation for the H62A mutant is particularly revealing given that the signal transmission has not been blocked, despite the perturbation of cofactor binding as evidenced by the low cofactor:protein stoichiometry and alteration of local structure caused by FAD modification and deletion of the side chain. The hydroxylation of the FAD is likely to result from the attack of the molecular oxygen residing near position 6, similar to the mechanism proposed for trimethylamine dehydrogenase based on an [18]O incorporation experiment (*48*). It is important to point out that the low FAD:protein stoichiometry observed for the proteins
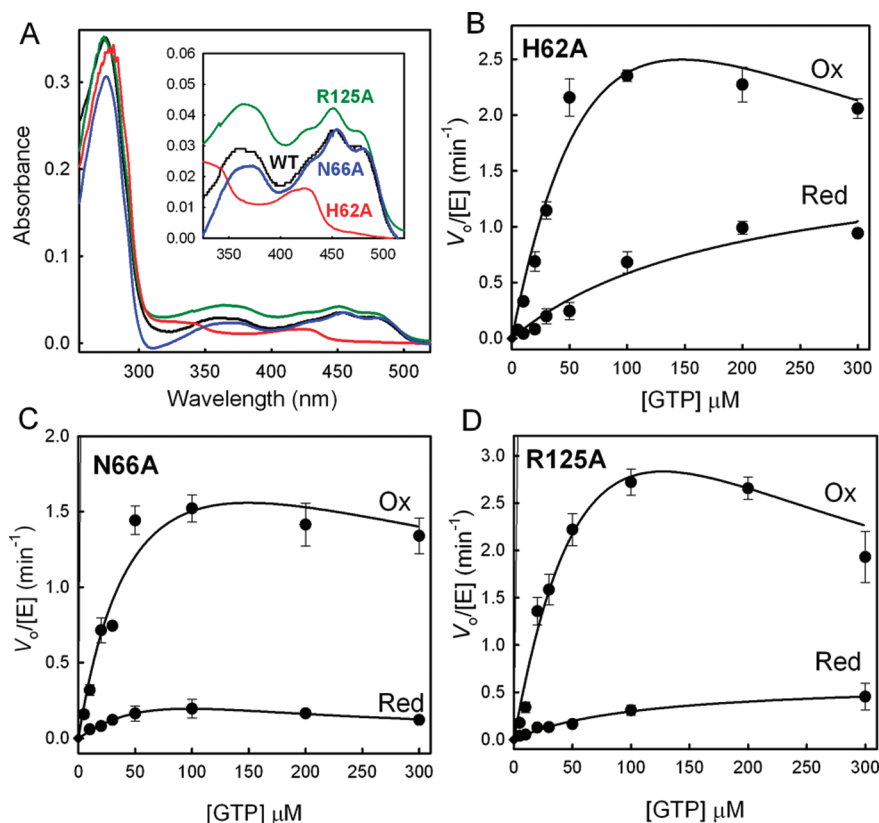
FIGURE 6: Comparison of *Ax*DGC2 and its mutants. (A) Absorption spectra of *Ax*DGC2 and the three mutants. (B−D) Comparison of the catalytic activity of the oxidized and reduced forms of the three *Ax*DGC2 mutants. Reaction buffer consisted of 100 mM Tris-HCl (pH 8.0), 50 mM KCl, and 10 mM MgCl$_2$.
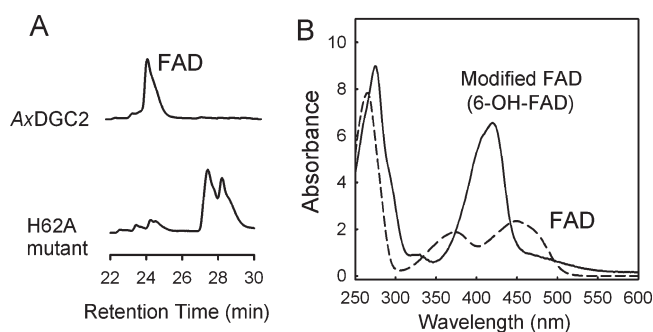

FIGURE 7: Modified FAD in mutant H62A. (A) Comparison of the HPLC chromatograms of FAD and the modified FAD from mutant H62A. (B) UV−vis spectra of FAD and the modified FAD from mutant H62A.

indicates that the protein solutions contain a large portion of apoprotein whose activity does not change with oxidation or reduction. Hence, the observed differences in catalytic rate between the reduced and oxidized proteins are likely to be even greater when the proteins are fully populated by the FAD. On the basis of these observations, we propose that substituted hydrogen-bonded water networks may form in the mutants, and that the protonation and deprotonation of the N5 atom can induce a structural change in the protein scaffold through the newly formed hydrogen-bonded water networks. As observed in the flavoprotein mandelate dehydrogenase, a change in the flavin redox state can be transmitted through an extensive hydrogen-bonded water network to induce conformational change (49). Nonetheless, the data do not completely rule out the possibility that the hydrogen-bonded network is still intact in the mutants.

Further structural study of the PAS$_{AvNifL}$ domain will reveal whether there are other residues for organization of the hydrogen-bonded network near the N5 atom and disclose the effect of the mutation on the local protein structure and the hydrogen-bonded network.

It should be emphasized that although the mutations did not totally disrupt the communication between the PAS and GGDEF domains, the three residues could still be crucial for the physiological function of the protein by affecting O$_2$ binding and electron transfer, and thus, the mutations may still be able to cause phenotypic changes. The binding of O$_2$ could be affected considering that O$_2$ must first bind near the N5 atom prior to the oxidation of the FAD (27). Rapid electron transfer between the PAS$_{AxDGC2}$ domain and its redox partners that include the oxidant O$_2$ and the unknown reductant is also critical for the fast response to the change in cellular redox status. Regardless of the identity of the redox partner, the rates of reduction and oxidation of *Ax*DGC2 will be dictated by the redox potential of the protein-embedded FAD (40, 50). In addition to the altered redox potential for the mutants, the reorganization energy that represents the kinetic barrier for electron transfer is likely to be affected as well given the perturbation of the environment in the FAD-binding pocket.

Intriguingly, the PDE activity assay revealed that although the EAL domain of *Ax*DGC2 did not degrade c-di-GMP under the experimental conditions, it is a competent PDE domain that can hydrolyze some phosphodiester bond-containing substrates. A one-metal ion catalytic mechanism for EAL domain proteins was proposed on the basis of the biochemical study on RocR (51), whereas the exquisite crystallographic study of Brbp1 recently suggested a two-metal ion mechanism (19).

Table 3: Redox Potentials of *Ax*DGC2 and Its Mutants

	wild type	H62A	N66A	R125A	AvNifL[a]	*Kp*NifL[b]	MmoS[c]
redox potential (mV)	-280 ± 3.0	-265 ± 1.3	-275 ± 0.8	-272 ± 2.3	-226 (pH 8.0)	-277 ± 5 (pH 8.0)	-291.2 (pH 8.0)

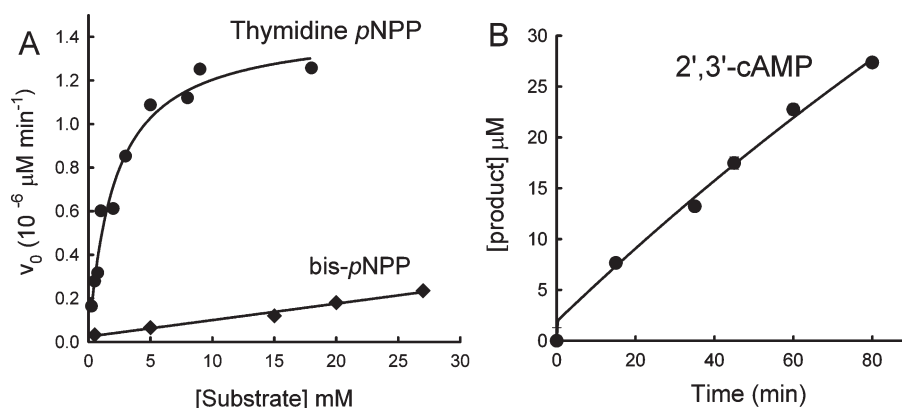[a]Data from ref *35*. [b]Data from ref *60*. [c]Data from ref *25*.

FIGURE 8: Catalytic activity of the EAL domain of *Ax*DGC2 toward nonphysiological phosphodiester substrates. (A) Hydrolysis of Bis-*p*-NPP and thymidine-*p*-NPP by *Ax*DGC2. (B) Hydrolysis of 2′,3′-cAMP by *Ax*DGC2 to produce 3′-AMP. Reaction conditions: 100 mM Tris-HCl (pH 8.0), 50 mM KCl, and 10 mM MgCl$_2$.

Considering the lack of an Asp residue for binding the second metal ion in *Ax*DGC2, the observed PDE activity seems to suggest that the EAL domain may use a one-metal ion mechanism for hydrolyzing the nitrophenol substrates and 2′,3′-cAMP/cGMP. Furthermore, the observation that the catalytic activity toward c-di-GMP can be recovered by restoring loop 6 also raised the possibility that the activity of the EAL domain toward c-di-GMP can be activated by an unidentified signal. A few bifunctional GGDEF−EAL didomain-containing proteins with catalytically active GGDEF and EAL domains have been documented (*52*, *53*). Interestingly, a recent study of ScrG, a GGDEF−EAL didomain protein in *Vibrio parahemolyticus*, showed that the protein exhibits DGC or PDE activity, depending on the presence of another protein partner (*54*). Hence, it remains to be seen whether *Ax*DGC2 is regulated by another signal in addition to the redox signal.

Finally, the study demonstrated that the change in the redox status of the flavin cofactor modulates the enzymatic activity of the GGDEF domain in *Ax*DGC2 and, thus, provided support for the notion that the FAD-containing PAS domain of *Ax*DGC2 functions as a redox and oxygen sensor. The PAS domains of *Ax*DGC1 and *Ax*DGC3 are likely to function as redox and oxygen sensors as well given the high degree of sequence similarity (>90%) shared by the PAS domains of *Ax*DGC1, -2, and -3. Considering that the estimated free cellular GTP concentration is in the range of 100−400 μM (*55*, *56*), the different rates observed for oxidized and reduced states could mirror the different efficiencies in degrading c-di-GMP for *Ax*DGC1, -2, and -3 in the cells. Together with an early study on *Ax*PDEA1 (*13*, *57*), the data would indicate that a high cellular O$_2$ concentration will simultaneously stimulate the DGC activity of *Ax*DGC1, -2, and -3 and suppress the PDE activity of *Ax*PDE1, -2, and -3, on the assumption that all six proteins are constitutively expressed. Consequently, the cellular c-di-GMP level will increase with oxygen concentration to enable the binding of c-di-GMP to the membrane-embedded cellulose synthase for activating cellulose synthesis (Figure 9). This model
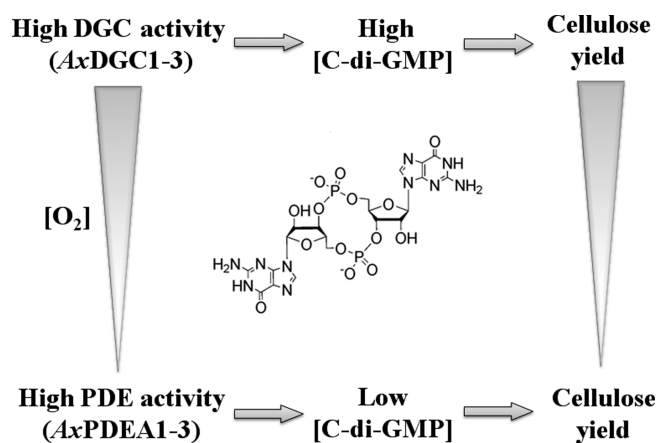

FIGURE 9: Schematic illustration of the relationship among oxygen level, cellular c-di-GMP concentration, and cellulose synthesis in *A. xylinum*.

is consistent with the observation that cellulose was produced by better aerated cells at the air−water interface in a static culture of *A. xylinum* (*13*, *46*). The utilization of flavin and heme-containing PAS domains for the synchronized regulation of DGC and PDE activities may be crucial for achieving a location-specific and fast O$_2$ response in the obligate aerobe *A. xylinum*.

SUPPORTING INFORMATION AVAILABLE

Additional sequence alignment, kinetic data, and redox potential titration plots. This material is available free of charge via the Internet at http://pubs.acs.org.

REFERENCES

1. Romling, U., and Amikam, D. (2006) Cyclic di-GMP as a second messenger. *Curr. Opin. Microbiol. 9*, 218–228.
2. Hengge, R. (2009) Principles of c-di-GMP signalling in bacteria. *Nat. Rev. Microbiol. 7*, 263–273.
3. Schirmer, T., and Jenal, U. (2009) Structural and mechanistic determinants of c-di-GMP signalling. *Nat. Rev. Microbiol. 7*, 724–735.

4. Simm, R., Morr, M., Kader, A., Nimtz, M., and Romling, U. (2004) GGDEF and EAL domains inversely regulate cyclic-di-GMP levels and transition from sessility to motility. *Mol. Microbiol. 53*, 1123–1134.

5. Romling, U., Gomelsky, M., and Galperin, M. Y. (2005) C-di-GMP: The dawning of a novel bacterial signalling system. *Mol. Microbiol. 57*, 629–639.

6. Galperin, M. Y. (2006) Structural classification of bacterial response regulators: Diversity of output domains and domain combinations. *J. Bacteriol. 188*, 4169–4182.

7. Galperin, M. Y., Nikolskaya, A. N., and Koonin, E. V. (2001) Novel domains of the prokaryotic two-component signal transduction systems. *FEMS Microbiol. Lett. 203*, 11–21.

8. Taylor, B. L., and Zhulin, I. B. (1999) PAS domains: Internal sensors of oxygen, redox potential, and light. *Mol. Biol. Rev. 63*, 479.

9. Hefti, M. H., Francoijs, K. J., de Vries, S. C., Dixon, R., and Vervoort, J. (2004) The PAS fold: A redefinition of the PAS domain based upon structural prediction. *Eur. J. Biochem. 271*, 1198–1208.

10. Gilles-Gonzalez, M.-A., and gonzalez, G. (2004) Signal transduction by heme-containing PAS-domain proteins. *J. Appl. Physiol. 96*, 774–783.

11. Wan, X., Tuckerman, J. R., Saito, J. A., Freitas, T. A. K., Newhouse, J. S., Denery, J. R., Galperin, M. Y., Gonzalez, G., Gilles-Gonzalez, M.-A., and Alam, M. (2009) Globins synthesize the second messenger bis-(3′-5′)-cyclic diguanosine monophosphate in bacteria. *J. Mol. Biol. 388*, 262–270.

12. Tuckerman, J. R., Gonzalez, G., Sousa, E. H. S., Wan, X., Saito, J. A., Alam, M., and Gilles-Gonzalez, M. A. (2009) An oxygen-sensing diguanylate cyclase and phosphodiesterase couple for c-di-GMP control. *Biochemistry 48*, 9764–9774.

13. Chang, A. L., Tuckerman, J. R., Gonzalez, G., Mayer, R., Weihouse, H., Volman, G., Amikam, D., Benziman, M., and Gilles-Gonzalez, M. A. (2001) Phosphodiesterase A1, a regulator of cellulose synthesis in *Acetobacter xylinum*, is a heme-based sensor. *Biochemistry 40*, 3420–3426.

14. Tanaka, A., Takahashi, H., and Shimizu, T. (2007) Critical role of the heme axial ligand, Met95, in locking catalysis of the phosphodiesterase from *Escherichia coli* (Ec DOS) toward cyclic diGMP. *J. Biol. Chem. 282*, 21301–21307.

15. Christie, J. M., Salomon, M., Nozue, K., Wada, M., and Briggs, W. R. (1999) LOV (light, oxygen, or voltage) domains of the blue-light photoreceptor phototropin (nph1): Binding sites for the chromophore flavin mononucleotide. *Proc. Natl. Acad. Sci. U.S.A. 96*, 8779–8783.

16. Moglich, A., and Moffat, K. (2007) Structural basis for light-dependent signaling in the dimeric LOV domain of the photosensor YtvA. *J. Mol. Biol. 373*, 112–126.

17. Gomelsky, M., and Klug, G. (2002) BLUF: A novel FAD-binding domain involved in sensory transduction in microorganisms. *Trends Biochem. Sci. 27*, 497–500.

18. Anderson, S., Dragnea, V., Masuda, S., Ybe, J., Moffat, K., and Bauer, C. (2005) Structure of a novel photoreceptor, the BLUF domain of AppA from *Rhodobacter sphaeroides*. *Biochemistry 44*, 7998–8005.

19. Barends, T. R. M., Hartmann, E., Griese, J. J., Beitlich, T., Kirienko, N. V., Ryjenkov, D. A., Reinstein, D. A., Shoeman, R. I., Gomelsky, M., and Schlichting, I. (2009) Structure and mechanism of a bacterial light-regulated cyclic nucleotide phosphodiesterase. *Nature 459*, 1015–1018.

20. Barry, L. T. (2007) Aer on the inside looking out: Paradigm for a PAS-HAMP role in sensing oxygen, redox and energy. *Mol. Microbiol. 65*, 1415–1424.

21. Hill, S., Austin, S., Eydmann, T., Jones, T., and Dixon, R. (1996) *Azotobacter vinelandii* NIFL is a flavoprotein that modulates transcriptional activation of nitrogen-fixation genes via a redox-sensitive switch. *Proc. Natl. Acad. Sci. U.S.A. 93*, 2143–2148.

22. Ukaegbu, U. E., and Rosenzweig, A. C. (2009) Structure of the redox sensor domain of *Methylococcus capsulatus* (Bath) MmoS. *Biochemistry 48*, 2207–2215.

23. Rebbapragada, A., Johnson, M. S., Harding, G. P., Zuccarelli, A. J., Fletcher, H. M., Zhulin, I. B., and Taylor, B. L. (1997) The Aer protein and the serine chemoreceptor Tsr independently sense intracellular energy levels and transduce oxygen, redox, and energy signals for *Escherichia coli* behavior. *Proc. Natl. Acad. Sci. U.S.A. 94*, 10541–10546.

24. Söderbäck, E., Reyes-Ramirez, F., Eydmann, T., Austin, S., Hill, S., and Dixon, R. (1998) The redox- and fixed nitrogen-responsive regulatory protein NIFL from *Azotobacter vinelandii* comprises discrete flavin and nucleotide-binding domains. *Mol. Microbiol. 28*, 179–192.

25. Ukaegbu, U. E., Henery, S., and Rosenzweig, A. C. (2006) Biochemical characterization of MmoS, a sensor protein involved in copper-dependent regulation of soluble methane monooxygenase. *Biochemistry 45*, 10191–10198.

26. Thummer, R., Klimmek, O., and Schmitz, R. A. (2007) Biochemical studies of *Klebsiella pneumoniae* NifL reduction using reconstituted partial anaerobic respiratory chains of *Wolinella succinogenes*. *J. Biol. Chem. 282*, 12517–12526.

27. Key, J., Hefti, M., Purcell, E. B., and Moffat, K. (2007) Structure of the redox sensor domain of *Azotobacter vinelandii* NifL at atomic resolution: Signaling, dimerization, and mechanism. *Biochemistry 46*, 3614–3623.

28. Tal, R., Wong, H. C., Calhoon, R., Gelfand, D., Fear, A. L., Volman, G., Mayer, R., Ross, P., Amikam, D., Weinhouse, H., Cohen, A., Sapir, S., Ohana, P., and Benziman, M. (1998) Three cdg operons control cellular turnover of cyclic di-GMP in *Acetobacter xylinum*: Genetic organization and occurrence of conserved domains in isoenzymes. *J. Bacteriol. 180*, 4416–4425.

29. Gonzalez, G., Dioum, E. M., Bertolucci, C. M., Tomita, T., Ikeda-Saito, M., Cheesman, M. R., Watmough, N. J., and Gilles-Gonzalez, M.-A. (2002) Nature of the displaceable heme-axial residue in the *Ec*Dos protein, a heme-based sensor from *Escherichia coli*. *Biochemistry 41*, 8414–8421.

30. Rao, F., Pasunooti, S., Ng, Y., Zhuo, W., Lim, L., Liu, W., and Liang, Z.-X. (2009) Enzymatic synthesis of c-di-GMP using a thermophilic diguanylate cyclase. *Anal. Biochem. 389*, 138–142.

31. Negri, A., Massey, V., and Williams, C. H., Jr. (1987) D-Aspartate oxidase from beef kidney. Purification and properties. *J. Biol. Chem. 262*, 10026–10034.

32. Arnold, K., Bordoli, L., Kopp, J., and Schwede, T. (2006) The SWISS-MODEL Workspace: A web-based environment for protein structure homology modelling. *Bioinformatics 22*, 195–201.

33. Wassmann, P., Chan, C., Paul, R., Beck, A., Heerklotz, H., Jenal, U., and Schirmer, T. (2007) Structure of BeF$_3^-$-modified response regulator PleD: Implications for diguanylate cyclase activation, catalysis, and feedback inhibition. *Structure 15*, 915–927.

34. De, N., Pirruccello, M., Krasteva, P. V., Bae, N., Raghavan, R. V., and Sondermann, H. (2008) Phosphorylation-independent regulation of the diguanylate cyclase WspR. *PLoS Biol. 6*, e67.

35. Macheroux, P., Hill, S., Austin, S., Eydmann, T., Jones, T., Kim, S. O., Poole, R., and Dixon, R. (1998) Electron donation to the flavoprotien NifL, a redox-sensing transcriptional regulator. *Biochem. J. 332*, 413–419.

36. Repik, A., Rebbapragada, A., Johnson, M. S., Haznedar, J. Q., Zhulin, I. B., and Taylor, B. L. (2000) PAS domain residues involved in signal transduction by the Aer redox sensor of *Escherichia coli*. *Mol. Microbiol. 36*, 806–816.

37. Jung, A., Domratcheva, T., Tarutina, M., Wu, Q., Ko, W. H., Shoeman, R. L., Gomelsky, M., Gardner, K. H., and Schlichting, L. (2005) Structure of a bacterial BLUF photoreceptor: Insights into blue light-mediated signal transduction. *Proc. Natl. Acad. Sci. U.S.A. 102*, 12350–12355.

38. Marshall, K. R., Gong, M., Wodke, L., Lamb, J. H., Jones, D. J. L., Farmer, P. B., Scrutton, N. S., and Munro, A. W. (2005) The human apoptosis-inducing protein AMID is an oxidoreductase with a modified flavin cofactor and DNA binding activity. *J. Biol. Chem. 280*, 30735–30740.

39. Igarashi, K., Verhagen, M. F. J. M., Samejima, M., Schulein, M., Eriksson, K.-E. L., and Nishino, T. (1999) Cellobiose dehydrogenase from the fungi *Phanerochaete chrysosporium* and *Humicola insolens*. A flavochemoprotein from *Humicola insolens* contains 6-hydroxy-FAD as the dominant active cofactor. *J. Biol. Chem. 274*, 3338–3344.

40. Davidson, V. L. (2000) What controls the rates of interprotein electron transfer reactions. *Acc. Chem. Res. 33*, 87–93.

41. Nocek, J. M., Zhou, J. S., Forest, S. D., Priyadarshy, S., Beratan, D. N., Onuchic, J. N., and Hoffman, B. M. (1996) Theory and practice of electron transfer within protein-protein complexes: Application to the multidomain binding of cytochrome *c* by cytochrome *c p*ceroxidase. *Chem. Rev. 96*, 2459–2489.

42. Liang, Z. X., Nocek, J. M., Kurnikov, I. V., Beratan, D. N., and Hoffman, B. M. (2000) Electrostatic control of electron transfer between myoglobin and cytochrome b_5: Effect of methylating the heme propionates of Zn-myoglobin. *J. Am. Chem. Soc. 122*, 3552–3553.

43. Zanetti, G., Massey, V., and Curti, B. (1983) FAD analogues as mechanistic and binding-domain probes of spinach ferredoxin-NADP$^+$ reductase. *Eur. J. Biochem. 132*, 201–205.

44. Rao, F., Qi, Y., Chong, H. S., Kotada, M., Li, B., Lescar, J., Tang, K., and Liang, Z.-X. (2009) The functional role of a conserved loop in

EAL domain-based c-di-GMP specific phosphodiesterase. *J. Bacteriol. 191*, 4722–4731.

45. Ross, P. (1987) Regulation of cellulose synthesis in *Acetobacter xylinum* by cyclic diguanylate. *Nature 325*, 279–281.

46. Ross, P., Mayer, R., Weinhouse, H., Amikam, D., Huggirat, Y., Benziman, M., de Vroom, E., Fidder, A., de Paus, P., and Sliedregt, L. A. (1990) The cyclic diguanylic acid regulatory system of cellulose synthesis in *Acetobacter xylinum*. Chemical synthesis and biological activity of cyclic nucleotide dimer, trimer, and phosphothioate derivatives. *J. Biol. Chem. 265*, 18933–18943.

47. Crosson, S., Rajagopal, S., and Moffat, K. (2003) The LOV domain family: Photoresponsive signaling modules coupled to diverse output domains. *Biochemistry 42*, 2–10.

48. Lu, X., Nikolic, D., Mitchell, D. J., van Breemen, R. B., Mersfelder, J. A., Hille, R., and Silverman, R. B. (2003) A mechanism for substrate-induced formation of 6-hydroxyflavin mononucleotide catalyzed by C30A trimethylamine dehydrogenase. *Bioorg. Med. Chem. Lett. 13*, 4129–4132.

49. Sukumar, N., Dewanti, A. R., Mitra, B., and Mathews, F. S. (2004) High resolution structures of an oxidized and reduced flavoprotein: The Water Switch in a Soluble Form of (S)-Mandelate Dehydrogenase. *J. Biol. Chem. 279*, 3749–3757.

50. Liang, Z. X., Nocek, J. M., Huang, K., Hayes, R. T., Kurnikov, I. V., Beratan, D. N., and Hoffman, B. M. (2002) Dynamic docking and electron transfer between Zn-myoglobin and cytochrome b_5. *J. Am. Chem. Soc. 124*, 6849–6859.

51. Rao, F., Yang, Y., Qi, Y., and Liang, Z. X. (2008) Catalytic mechanism of c-di-GMP specific phosphodiesterase: A study of the EAL domain-containing RocR from *Pseudomonas aeruginosa. J. Bacteriol. 190*, 3622–3631.

52. Tarutina, M., Ryjenkov, D. A., and Gomelsky, M. (2006) An unorthodox bacteriophytochrome from *Rhodobacter sphaeroides*

involved in turnover of the decond messenger c-di-GMP. *J. Biol. Chem. 281*, 34751–34758.

53. Kumar, M., and Chatterji, D. (2008) Cyclic-di-GMP: A second messenger required for long-term survival, but not for biofilm formation, in *Mycobacterium smegmatis. Microbiology 154*, 2942–2955.

54. Kim, Y.-K., and McCarter, L. L. (2007) ScrG, a GGDEF-EAL protein, participates in regulating swarming and sticking in *Vibrio parahaemolyticus. J. Bacteriol. 189*, 4094–4107.

55. Buchholz, A., Takors, R., and Wandrey, C. (2001) Quantification of intracellular metabolites in *Escherichia coli* K12 using liquid chromatographic-electrospray ionization tandem mass spectrometric techniques. *Anal. Biochem. 295*, 129–137.

56. Hatakeyama, K., Harada, T., and Kagamiyama, H. (1992) IMP dehydrogenase inhibitors reduce intracellular tetrahydrobiopterin levels through reduction of intracellular GTP levels. Indications of the regulation of GTP cyclohydrolase I activity by restriction of GTP availability in the cells. *J. Biol. Chem. 267*, 20734–20739.

57. Green, J., and Pager, M. (2004) Bacterial redox sensors. *Nat. Rev. Microbiol. 2*, 954–966.

58. Bibikov, S. I., Barnes, L. A., Gitin, Y., and Parkinson, J. S. (2000) Domain organization and flavin adenine dinucleotide-binding determinants in the aerotaxis signal transducer Aer of *Escherichia coli. Proc. Natl. Acad. Sci. U.S.A. 97*, 5830–5835.

59. Masuda, S., Hasegawa, K., Ishii, A., and Ono, T. A. (2004) Light-induced structural changes in a putative blue-light receptor with a novel FAD binding fold sensor of blue-light using FAD (BLUF): Slr1694 of *Synechocystis sp*. PCC6803. *Biochemistry 43*, 5304–5313.

60. Klopprogge, K., and Schmitz, R. A. (1999) NifL of K*lebsiella pneumoniae:* Redox characterization in relation to the nitrogen source. *Biochim. Biophys. Acta 1431*, 462–470.